Rodlike molecules in extreme confinement

Xiaomei Yao
School of Chemistry, Beihang University, Beijing 100191, People's Republic of China

Jeff Z. Y. Chen*
Department of Physics and Astronomy, University of Waterloo, Waterloo, Ontario, Canada N2L 3G1

(Received 14 February 2020; accepted 15 June 2020; published 29 June 2020)

A unique feature of colloid particles and biopolymers is the molecule's intrinsic rigidity characterized by a molecular-level length scale. Under extreme confinement conditions at cellular scales or in nanodevices, these molecules can display orientational ordering accompanied by severe density depletion. Conventional liquid-crystal theories, such as the Oseen-Frank or Landau–de Gennes theories, cannot capture the essential molecular-level properties: the boundary effects, which extend to a distance of the rigidity length scale, and the drastic variations of the inhomogeneous molecular density. Here we show, based on a simple interpretation of the Onsager model, that rodlike molecules in extreme annular confinement produce unusual liquid-crystal defect structures that are independent phases from the patterns usually seen in a weaker confinement environment.

DOI: 10.1103/PhysRevE.101.062706

I. INTRODUCTION

The fluid formed by rodlike molecules is a model system of liquid crystals, which is often considered in computer simulations. Closely related real systems are micron-sized colloidal silica rods [1] or visible-range granular rods [2,3] that display the typical behavior of lyotropic liquid crystals: the formation of a nematic state when the particle density is sufficiently high and the exhibition of defect patterns when the orientationally ordered system is confined in a finite space. A prominent feature of biopolymers and colloid particles is the molecule's intrinsic rigidity characterized by a molecular-level length scale. Recent experimental systems include aqueous suspensions of actin filaments [4] and linearly shaped viruses [5] confined in a microchamber. How does the finite geometric confinement affect the orientational properties and local molecular densities of a liquid crystal made of molecules that have sizes competing with the confinement length scale?

One might say that this question is already answered by the recent progress in liquid-crystal physics. The subject of liquid-crystal defects caused by geometric frustrations has been one of the central focuses in the liquid-crystal research community in recent years. The defect morphologies appearing in single and double liquid-crystal emulsions [6,7], liquid-crystal display cells [8], as well as confined semiflexible biomolecules [4,5] are excellent experimental examples. The molecular-level computer simulations produced defect patterns under various physical conditions [9–16] that furthered our understanding of the nature of the defects. Most theoretical studies in this research area [15,17–35] are based on the Oseen-Frank (OF) model or the Landau–de Gennes (LdG) model, where the nematic director field or the Q-tensor field [36] are the main concerns, respectively. These coarse-grained models, in which the molecular individuality is mostly ignored, are suitable for dealing with liquid crystals made of small molecules.

The case of liquid crystals under extreme confinement is outside the realm of the conventional OF or LdG models, when the molecular size is comparable with the confinement dimension. Here the nonlocal boundary effects can extend to a significant distance covering a several rigidity length scale. Such a key physical feature cannot be described by the OF and LdG theories, as they are models for local order parameters. An excellent example is rodlike molecules, each having length L, confined in the annular area formed by two concentric circles of radii R_1 and R_2, as illustrated in Fig. 1. Recent experiment observations and computer simulations revealed molecular configurations that are unique to such finite-sized systems [14]. The excluded-volume interaction between rods prefers mutually parallel alignment of the rod axes. In an ideal bulk state without a border, this drives the molecules into the formation of a directionally ordered, but spatially homogeneous nematic state at a sufficiently high particle density. The hard annular boundaries disrupt the uniform nematic order and produce defect states in the interior. Depending on the geometric ratios R_2/L and R_1/R_2, molecular configurations display multiple stable states, each characterized by particular rotational symmetries.

Can we understand the stability of these states from a theoretical model? The OF model deals with a continuous, nematic director field, and the LdG model deals with a continuous, Q-tensor field, in which two crucial mechanisms required for the current problem are lacking: a rod cannot cross any hard-wall boundaries, illustrated in Fig. 1(b), and the density depletion caused by such a boundary condition (BC) produces an entropy cost to the free energy. Hence, we need another level of coarse graining, i.e., a free-energy model that contains

*jeffchen@uwaterloo.ca

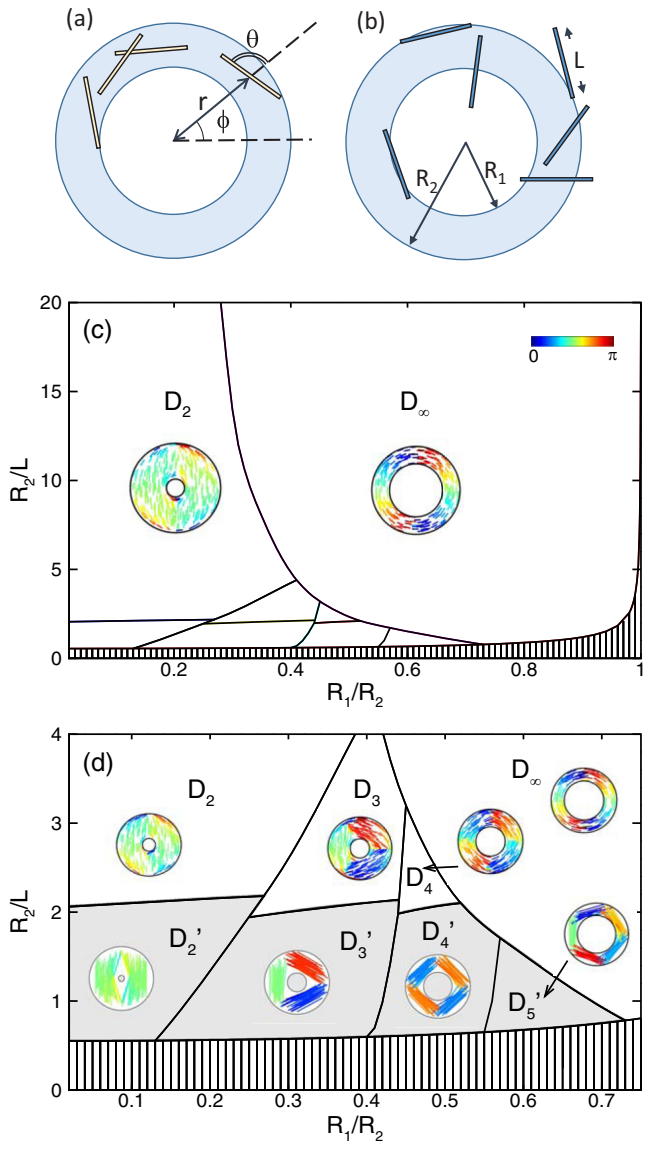

FIG. 1. Rodlike molecules of length L confined in concentric annular circles of radii R_1 and R_2. (a),(b) Typical allowed (yellow) and disallowed (blue) configurations, realized in our theory. (c) Two phase regimes which exist when $R_2/L \gg 1$: a twofold defect state (D_2) and a uniform defect-free state (D_∞), divided by a phase boundary. Multiple states exist in the extreme confinement region of $R_2/L \sim 1$, as illustrated in phase diagram (d), based on the numerical solution of the extended Onsager free energy for interacting, rodlike molecules. An overall number density of rods, $\rho_0 = 20/L^2$, is assumed here, where ρ_0 is the number of rods per unit area on a two-dimensional surface. The phase boundaries are determined by a comparison of the free energies. The color of the rods illustrated in (c) and (d) represents the angles that the rods make with respect to the horizontal axis, specified in the inset of (c). The shaded area is defined in Appendix B.

a continuous field variable and yet allows for specification of BCs at a molecular level.

In 1949, Onsager proposed an idea for studying the orientational properties of rodlike molecules [37]. The purpose of this paper is twofold: to demonstrate that the extended version of the Onsager model fits into this requirement, and, to provide a quantitative analysis of the annular confinement problem. The extended Onsager model treats the problem at a different level: the consideration is the molecular distribution density, not the continuum local nematic director or the Q-tensor fields. When the numerical analysis is done, we show that a unique set of extreme-confinement states emerge, which is different from the defect states predicted from the conventional OF or LdG models.

II. THEORETICAL APPROACH

Our focus is on the distribution density function $\rho_c(\mathbf{r}, \mathbf{u})$ in a flat two-dimensional (2D) space. It characterizes the probability density of finding the centers of mass of rodlike molecules at a spatial position specified by the vector $\mathbf{r}$, with the condition that the rods point at the direction specified by the unit vector $\mathbf{u}$. The normalization condition $\int d\mathbf{r} \int d\mathbf{u} \rho_c(\mathbf{r}, \mathbf{u}) = n$ is assumed here, where n is the total number of confined rodlike molecules in an area A. We follow Onsager's approach [37] to write the free energy of the system by using a Mayer expansion accurate to the second virial term [38],

$$\beta F = \int \rho_c(\mathbf{r}, \mathbf{u}) \ln[L^2 \rho_c(\mathbf{r}, \mathbf{u})] d\mathbf{r} d\mathbf{u} + \frac{1}{2} \int \rho_c(\mathbf{r}, \mathbf{u}) w(\mathbf{r}, \mathbf{u}; \mathbf{r}', \mathbf{u}') \rho_c(\mathbf{r}', \mathbf{u}') \, d\mathbf{r} d\mathbf{u} d\mathbf{r}' d\mathbf{u}', \tag{1}$$

where $\beta = 1/k_B T$, with k_B being the Boltzmann constant and T the temperature. The free energy includes two terms. The first term takes into account the translational, density-depletion, and orientational entropies of a spatially inhomogeneous and orientationally ordered fluid of rodlike molecules. The second term describes the interaction between two rodlike molecules having the coordinates $(\mathbf{r}, \mathbf{u})$ and $(\mathbf{r}', \mathbf{u}')$, where the Mayer function $-w = \exp(-\beta v) - 1$, and v is the interaction potential energy between the two rigid molecules. When the configuration $(\mathbf{r}, \mathbf{u}; \mathbf{r}', \mathbf{u}')$ makes two rods overlapping, $v = \infty$; otherwise, $v = 0$. On a 2D surface, the mathematical criterion for determining rod overlapping becomes simple. The vectors $\mathbf{r}$ and $\mathbf{u}$ are represented by the variables (r, φ) and θ, respectively [Fig. 1(a)].

The reduced free energy βF as a functional of the function $\rho_c(\mathbf{r}, \mathbf{u})$ needs to be minimized. The stationary solutions satisfy

$$\frac{\delta F}{\delta \rho_c(\mathbf{r}, \mathbf{u})} = 0. \tag{2}$$

In a spatially homogeneous system where $\rho_c(\mathbf{r}, \mathbf{u})$ is actually a function of $\mathbf{u}$ only, one can analytically show that based on this requirement, the isotropic-nematic phase transition takes place when the 2D particle density $\rho_0 = n/A$ reaches a critical $\rho_0^* = 3\pi/(2L^2)$ [39–41]. For the current confined case where ρ_c is a function of both $\mathbf{r}$ and $\mathbf{u}$, we established a high-precision computational procedure, required to solve the above condition and to calculate the free energy. We refer to Ref. [42] for the detailed numerical procedure, which was established based on the equivalent self-consistent field theory of polymers [43,44].

III. VISUALIZATION OF THE STRUCTURES

In the following, a number of physical properties are analyzed and displayed, calculated from the distribution function of the center of mass of a rodlike molecule, $\rho_c(r, \varphi; \theta)$, obtained from minimizing the free energy. The center-of-mass molecular density, for example, is represented by

$$\Phi_c(r, \varphi) = \frac{1}{\rho_0} \int_0^{2\pi} \rho_c(r, \varphi, \theta) d\theta, \tag{3}$$

which is plotted in Fig. 2.

One can deduce the distribution density function for segments on the rodlike molecules, regardless of the position on the rod, by defining

$$f(\mathbf{r}, \mathbf{u}) = \frac{1}{\rho_0} \int_0^1 \rho_c \left[\mathbf{r} - \mathbf{u} L \left(s - \frac{1}{2} \right), \mathbf{u} \right] ds, \tag{4}$$

where the distribution of the segments at the path coordinate s is traced back to the rod center. The integrant represents the probability density of finding the segment labeled by s on the rodlike molecule to appear at a location with the coordinate $\mathbf{r}$. With this definition, $f(\mathbf{r}, \mathbf{u})$ is dimensionless and $\int d\mathbf{r} \int d\mathbf{u} f(\mathbf{r}, \mathbf{u}) = A$.

A number of properties are calculated by using $f(\mathbf{r}, \mathbf{u})$. The distribution density function for rod segments is calculated from

$$\phi(r, \varphi) = \int_0^{2\pi} f(r, \varphi, \theta) d\theta, \tag{5}$$

which is plotted in Appendix A. The 2×2 Q-tensor,

$$\mathsf{Q}(r, \varphi) = \frac{1}{2} \begin{bmatrix} S(r, \varphi) & T(r, \varphi) \\ T(r, \varphi) & -S(r, \varphi) \end{bmatrix}, \tag{6}$$

is calculated from

$$S(r, \varphi) = \frac{\int_0^{2\pi} d\theta \cos(2\theta) f(r, \varphi, \theta)}{\phi(r, \varphi)}, \tag{7}$$

$$T(r, \varphi) = \frac{\int_0^{2\pi} d\theta \sin(2\theta) f(r, \varphi, \theta)}{\phi(r, \varphi)}. \tag{8}$$

Both S and T characterize the orientational ordering of the rodlike molecules by themselves and can be used directly. The scalar orientational order parameter is determined by the positive eigenvalue of the Q-tensor,

$$\Lambda(r, \varphi) = \sqrt{S^2(r, \varphi) + T^2(r, \varphi)}, \tag{9}$$

which is plotted in Fig. 2. Particularly, the locations where $\Lambda \to 0$ are considered as defect points.

The nematic-director field itself is projected on the polar coordinates by

$$\mathbf{n}(r, \varphi) = \cos\theta_0(r, \varphi) \mathbf{e}_r + \sin\theta_0(r, \varphi) \mathbf{e}_\varphi, \tag{10}$$

where θ_0 is determined from

$$\cos\theta_0(r, \varphi) = \frac{1}{2} \left[1 + \frac{S(r, \varphi)}{\Lambda(r, \varphi)} \right]. \tag{11}$$

The unit vectors $\mathbf{e}_r$ and $\mathbf{e}_\varphi$ are those associated with the definition of the polar coordinates r, φ. We can then assess

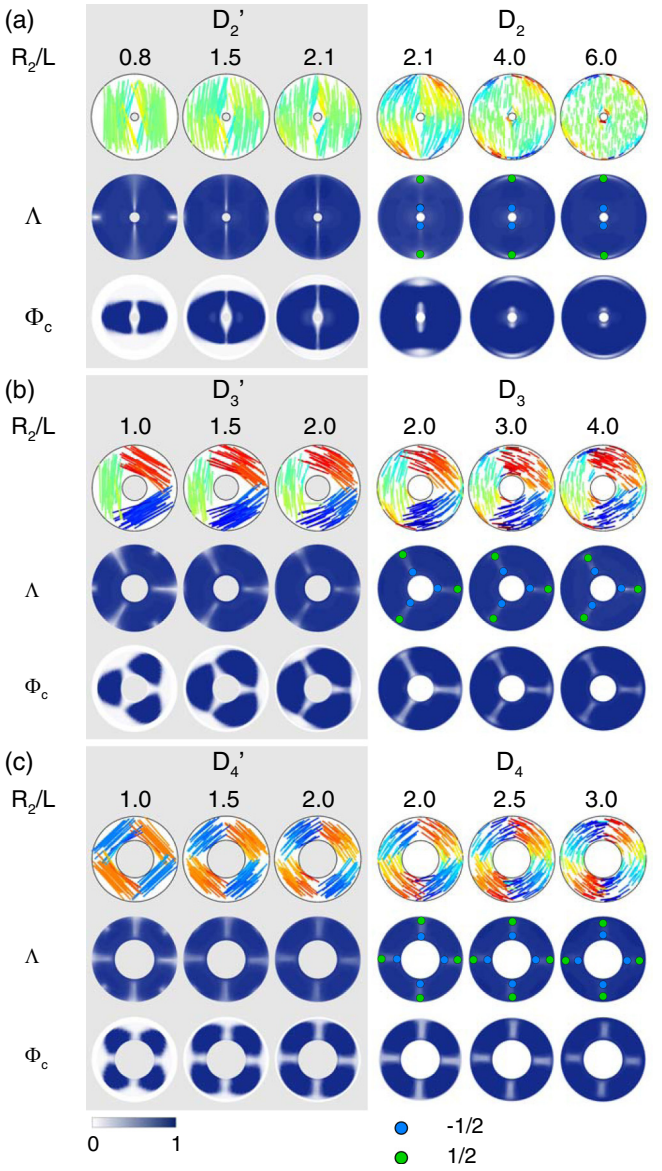

FIG. 2. Defect structures under the extreme confinement condition. Three illustration methods are used, all based on the numerical solution of $\rho_c(\mathbf{r}, \mathbf{u})$. The first row in each plot is a reconstructed, real-space illustration; the second row is the scalar orientational order parameter, calculated from the distribution function; and the third row is the center-of-mass distribution function, after averaging over all orientations. The first-order phase boundaries separating D_m from D'_m are represented by the change of the background shades: from white to light gray, where $m = 2$, 3, and 4 in (a) $R_1/R_2 = 0.1$, (b) $R_1/R_2 = 0.3$, and (c) $R_1/R_2 = 0.45$, respectively. The color used in the first row of each plot has the same meaning as in the inset of Fig. 1(c). The intensities of both Λ and Φ_c are represented by the blue color bar. The light-blue and green circles indicate the defect locations on D_m, of $-1/2$ and $1/2$ winding numbers, respectively.

the variance of the angle θ_0 at $r = R_2$,

$$\sigma^2 = \int_0^{2\pi} \theta_0^2(R_2, \varphi) d\varphi - \left[\int_0^{2\pi} \theta_0(R_2, \varphi) d\varphi \right]^2, \tag{12}$$

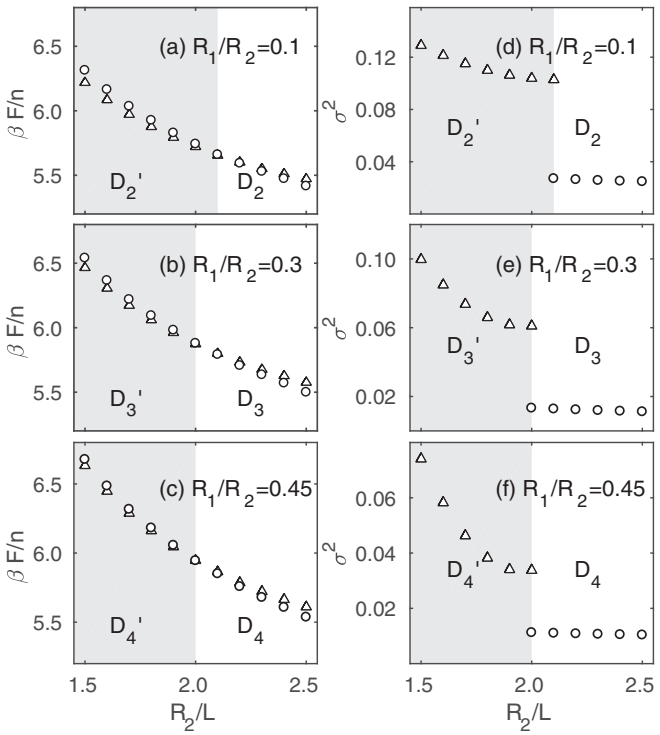

FIG. 3. Phase transitions between D'_m and D_m. For each case of (a) $m = 2$, (b) $m = 3$, and (c) $m = 4$, two branches of the reduced free energy per rod, triangles for D'_m and circles for D_m, are plotted in (a)–(c). The variance of the nematic direction at $r = R_2$, σ^2, is used as the order parameter of the D'_m-D_m transitions and displayed in (d)–(f) for $m = 2$, $m = 3$, and $m = 4$, respectively. Jumps of σ^2 can be seen at the transition points.

which is used in Fig. 3 as the order parameter for the D'_m phases.

To simulate the defect patterns seen by the cross-polarizer experiments, the first polarizer is assumed to make an angle α with respect to the x axis in the Cartesian coordinates used to illustrate the defect patterns. After the light passes through the liquid-crystal cell, the outcome of the light intensity is proportional to

$$I_\alpha(r,\varphi) = \frac{1}{4}\int_0^{2\pi} d\theta[\sin(2\varphi + 2\theta - 2\alpha)]^2 f(r,\varphi,\theta), \quad (13)$$

which is illustrated below.

IV. RESULTS

A. Boundary-driven phase separation

Note that we implemented the steric hard-wall BCs, which forbid the example configurations illustrated in Fig. 1(b), with no further assumptions of density function $\rho_c(\mathbf{r},\mathbf{u})$ at the boundaries. The BCs amount to letting the density $\rho_c(\mathbf{r},\mathbf{u})$ vanish when a rod, having coordinates $(\mathbf{r},\mathbf{u})$, overlaps with any part of the two concentric circles. This nonlocal interaction has a correlation length of order L, which cannot be ignored when R_1, R_2, and L become comparable. The second, nonlocal term in (1) connects the density function at different locations. After solving the minimization condition in (2) for the entire $(\mathbf{r},\mathbf{u})$ space, we can then deduce the normalized density function $\Phi_c(\mathbf{r})$ by averaging over all directions, and the $\mathsf{Q}(\mathbf{r})$-tensor for any $\mathbf{r}$. The eigenvalues and eigenvectors of the Q-tensor also yield the scalar orientational order parameter $\Lambda(\mathbf{r})$ and the main-axis nematic director $\mathbf{n}(\mathbf{r})$.

The numerical solution reveals the existence of two different types of defect states, D_m and D'_m, each displaying an m-fold rotational symmetry (Fig. 1), where $m = 2, 3, 4, \ldots$. The extreme defect states D'_m are characteristically identified to have the strong presence of self-aggregation of the center of mass (Fig. 2). Accompanying the density-depleted *regions* are weakly ordered rod segments, which can be compared with a much clearer signal of defect *points* in D_m. At a low R_2/L ratio, the geometric frustrations due to the BCs reduce the available free space for the rodlike molecules and effectively drive up the excluded-volume effects; rich domains of rod centers with orientationally ordered configurations reduce the overall excluded-volume effects, at the expense of unwanted reduction of the translational entropy in the polar-angle direction.

In addition to these effects, at the inner and outer circular boundaries, the configurational properties of D'_m significantly differ from those of D_m. At $r = R_2$ and $r = R_1$, both $\Lambda(r,\varphi)$ and $\mathbf{n}(r,\varphi)$ vary as functions of φ and the variation becomes stronger as R_2/L decreases, under extreme confinement. In contrast, these boundary properties remain at almost constant values in D_m. In a typical treatment of the LdG theory for a confinement problem, $\Phi_c(\mathbf{r})$ is assumed to be a constant over the entire confined space; at the boundaries, $\Lambda(r,\varphi)$ is assumed to be a constant and $\mathbf{n}(r,\varphi)$ to point at a constant angle from the boundary tangent direction. Indeed, a LdG theory can describe the D_2, D_∞, and spiral states [32,33].

B. Phase transitions

The fact that D'_m and D_m are different defect phases can be assessed from the free-energy branches of these two types of states. Displayed on the left panels of Fig. 3 are the typical free energies of these states, where $R_1/R_2 = 0.1$ for $m = 2$ in Fig. 3(a), 0.3 for $m = 3$ in Fig. 3(b), and 0.45 for $m = 4$ in Fig. 3(c). The plots clearly show how the D'_m and D_m branches cross each other at the transition points, as R_2/L varies. These and other crossing points (not displayed in Fig. 3) are used for the final determination of the first-order phase boundaries in the phase diagrams, shown by Figs. 1(c) and 1(d). Through the eigenvectors of the deduced Q-tensor at $r = R_2$, we calculate the nematic angle at the boundary. The variance of this angle, σ^2, can be used as the order parameter for this transition, as displayed in Figs. 3(d)–3(f). The jumps at the transition points clearly indicate the strong variations of the nematic angles in the D'_m states.

In a continuous vector field, a winding number can be assigned to a field-defect *point*. As a general rule, the total sum of the winding numbers in a given geometry is assumed conservative [17,45–47]. One can argue, e.g., that the annuler confinement amounts to a total winding number zero, and the circular confinement total winding number $+1$ [42]. Indeed, the ideal annular D_∞ is a state without any defect. The continuous D_m states contain m pairs of defect points that can be assigned positive and negative winding numbers (see

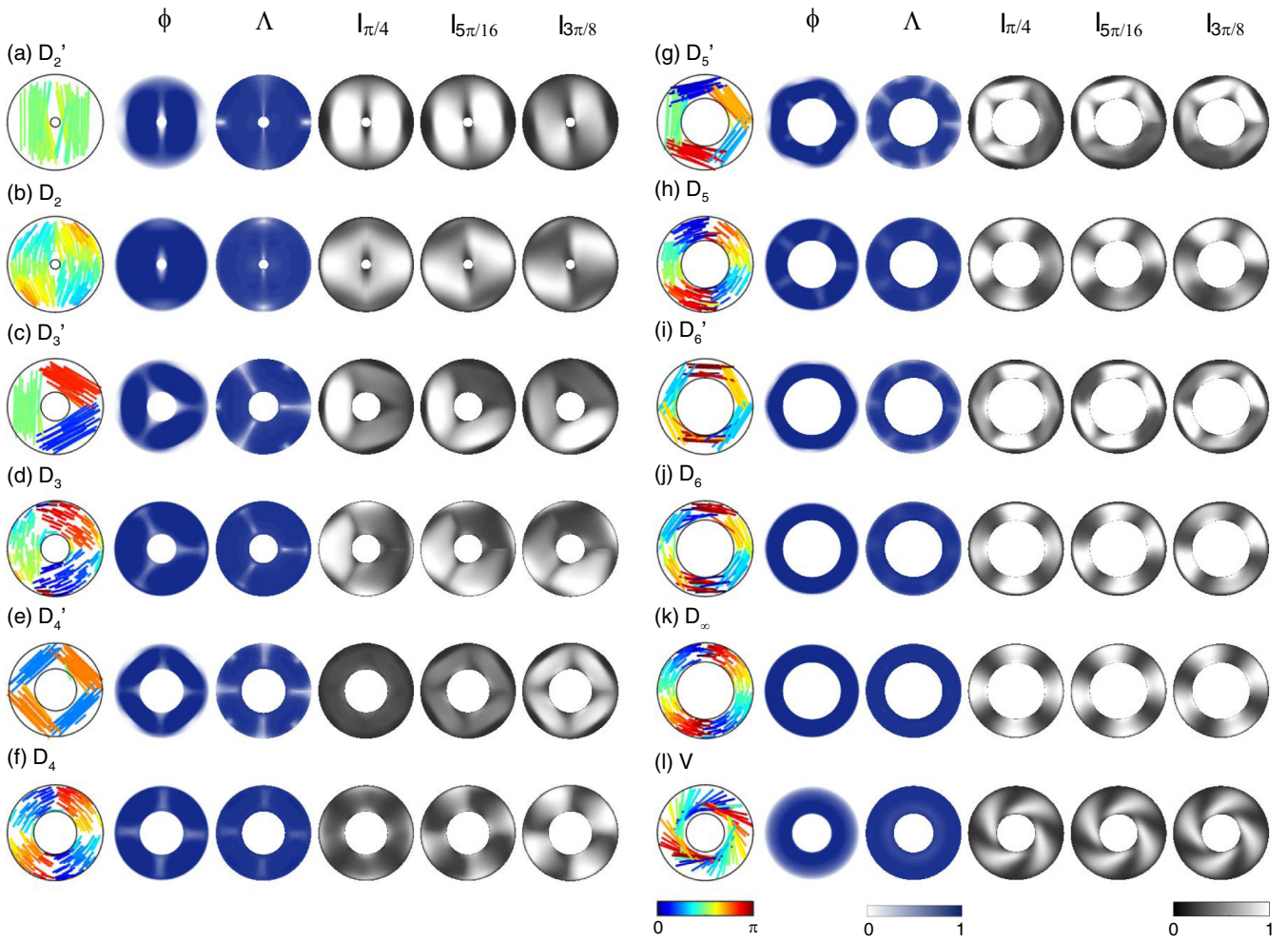

FIG. 4. All topologically different states found from our solutions to the extended Onsager model for the current geometry. Some of them show up in the phase diagrams, shown in Figs. 1(c) and 1(d). The snapshots in the first column illustrate the positions of the rods and their orientations, where the color represents the angle of a rod with respect to the horizontal axis specified by the color bar. For easy reference, we produce simulated cross-polarizer images of these states, I_α ($\alpha = \pi/4$, $5\pi/16$, and $3\pi/8$), according to (13), where α is the angle between the first polarizer direction and the horizontal axis of these plots.

Fig. 2), and hence the total winding number is still zero. The $-1/2$ defect points, labeled in Fig. 2 by the blue color, appear near the inner circle. As the ratio R_1/R_2 decreases, these $-1/2$ defect points are attracted to the vicinity of the inner circle, which has an increasing curvature (another property of liquid-crystal defect points [45]). This is consistent with the observation from Monte Carlo simulations [14]. As R_1/R_2 goes to zero, the annular confinement approaches the limit of a circular confinement of radius R_2. The two $-1/2$ defect points in the D_2 state diminish together with the inner circle, leaving a total winding number $m/2 = +1$ for $m = 2$, expected for the circular confinement [42,43]. This crossover requirement alone establishes the fact that the low-R_1/R_2 D_m state must be D_2, not another m.

Although the density functions $\rho_c(\mathbf{r}, \mathbf{u})$ of the extreme D'_m states are continuous, they vary drastically in both $\mathbf{r}$- and $\mathbf{u}$-variable spaces. This makes the orientational-configuration variation almost disruptive, as can be seen in the left panels of Fig. 2. As a result, significant *regions* of $\Lambda = 0$ appear in the order parameter profile, where the concept of defect *points* becomes irrelevant. In a recent theoretical study of a semiflexible polymer chain confined in a spherical cavity, a density-depletion region is also found under the extreme-confinement condition, when the confinement dimension has the same order of magnitude as the persistence length of the polymer [48]. This places the applicability of the general theory of defect *points* in question, on the extreme defect states.

There are two types of steric-repulsion effects in the current model. One is the boundary effects that completely forbid typical configurations, illustrated in Fig. 1(b). A long rod (small R_2/L) cannot fit into the interior of the annular geometry, which determines the lower bound of the phase diagram in Fig. 1(c) (see Appendix B). The other type is due to the Mayer function $-w$. While $v = +\infty$ when two rods overlap, illustrated by an example configuration in Fig. 1(a), the Mayer function allows the configuration but with a "soft" energy penalty $w = 1$, appearing in Eq. (1). As such, the Mayer function more appropriately approximates a thin, 2D-like layer of rodlike molecules. In some extreme states, the continuum Φ_c varies drastically crossing depletion and nondepletion regions, but is still continuous due to the soft penalty.

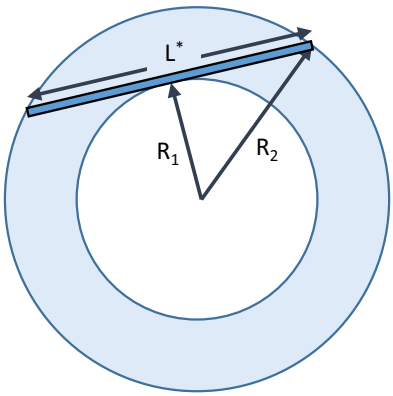

FIG. 5. Illustration of the limit of the rod length, L^*, which allows the rod to just fit into the annular confinement.

V. SUMMARY

A distinct feature of the Onsager model is its simplicity: a term describing entropy and a term describing the excluded-volume interaction. The original model was proposed to describe the bulk isotropic-nematic transition. Yet, the extended version to include the spatial variation expands much beyond the original model—it can be used to describe much more complicated, liquid-crystal problems of current interest. [42,43,49–52].

Here we demonstrate its capability to describe the physics of extreme confinement through nonlocal boundary conditions, which the conventional Oseen-Frank and Landau–de Gennes models fail to capture [32,33]. A rich phase diagram is obtained—not only are the states of different rotational symmetries separated by phase-transition boundaries, but two separate phases of the same symmetry are identified. Our free-energy calculation provides a theoretical foundation to establish the liquid-crystal properties under extreme annular confinement, for which Monte Carlo configurations were recently reported [14].

ACKNOWLEDGMENTS

The authors wish to acknowledge the financial support from the Postdoctoral Science Foundation of China (Grant No. 2019M660386), National Natural Science Foundation of China (Grant No. 21873009), and Natural Sciences and Engineering Research Council of Canada.

APPENDIX A: STATIONARY SOLUTIONS

In the main text, we presented our solutions from minimization of the free energy, which produce the defect profiles D_m, where $m = 2, 3, 4$, and ∞, and D'_m, where $m = 2, 3, 4$, and 5. Additional profiles, containing rotational symmetries up to $m = 6$, are also found from our numerical solutions, as illustrated in Fig. 4. Notably, a spiral, defect-free configuration V can be stabilized when $R_1/R_2 \lesssim 0.5$. These additional states could be metastable defect patterns, but have higher free energies in comparison with those of the states plotted in Fig. 1 of the main text.

APPENDIX B: LOWER BOUND IN FIG. 1

In the main text, Figs. 1(c) and 1(d) contain a shaded region where no possible states exist in the phase diagrams. The boundary is determined by the consideration of the geometry shown in Fig. 5, which yields

$$\frac{R_2}{L^*} = \frac{1}{2\sqrt{1-(R_1/R_2)^2}}. \tag{B1}$$

Here, the rod thickness is ignored. Below R_2/L^*, no rigid rodlike molecules can fit into the confinement geometry.

[1] L. B. G. Cortes, Y. Gao, R. P. A. Dullens, and D. G. A. L. Aarts, J. Phys.: Condens. Matter **29**, 064003 (2017).
[2] J. Galanis, D. Harries, D. L. Sackett, W. Losert, and R. Nossal, Phys. Rev. Lett. **96**, 028002 (2006).
[3] J. Galanis, R. Nossal, W. Losert, and D. Harries, Phys. Rev. Lett. **105**, 168001 (2010).
[4] M. Soares e Silva, J. Alvarado, J. Nguyen, N. Georgoulia, B. M. Mulder, and G. H. Koenderink, Soft Matter **7**, 10631 (2011).
[5] A. H. Lewis, I. Garlea, J. Alvarado, O. J. Dammone, P. D. Howell, A. Majumdar, B. M. Mulder, M. P. Lettinga, G. H. Koenderink, and D. G. A. L. Aarts, Soft Matter **10**, 7865 (2014).
[6] A. Fernández-Nieves, V. Vitelli, A. S. Utada, D. R. Link, M. Márquez, D. R. Nelson, and D. A. Weitz, Phys. Rev. Lett. **99**, 157801 (2007).
[7] T. Lopez-Leon, V. Koning, K. B. S. Devaiah, V. Vitelli, and A. Fernandez-Nieves, Nat. Phys. **7**, 391 (2011).
[8] C. Tsakonas, A. J. Davidson, C. V. Brown, and N. J. Mottram, Appl. Phys. Lett. **90**, 111913 (2007).
[9] J. Dzubiella, M. Schmidt, and H. Löwen, Phys. Rev. E **62**, 5081 (2000).
[10] H. Shin, M. J. Bowick, and X. Xing, Phys. Rev. Lett. **101**, 037802 (2008).
[11] M. A. Bates, J. Chem. Phys. **128**, 104707 (2008).
[12] D. de las Heras, E. Velasco, and L. Mederos, Phys. Rev. E **79**, 061703 (2009).
[13] T. Geigenfeind, S. Rosenzweig, M. Schmidt, and D. de las Heras, J. Chem. Phys. **142**, 174701 (2015).
[14] I. C. Gârlea, P. Mulder, J. Alvarado, O. Dammone, D. G. A. L. Aarts, M. P. Lettinga, G. H. Koenderink, and B. M. Mulder, Nat. Commun. **7**, 12112 (2016).
[15] M. Robinson, C. Luo, P. E. Farrell, R. Erban, and A. Majumdar, Liq. Cryst. **44**, 2267 (2017).
[16] A. Nikoubashman, D. A. Vega, K. Binder, and A. Milchev, Phys. Rev. Lett. **118**, 217803 (2017).
[17] T. C. Lubensky and J. Prost, J. Phys. II (France) **2**, 371 (1992).
[18] D. R. Nelson, Nano Lett. **2**, 1125 (2002).
[19] M. Huber and H. Stark, Europhys. Lett. **69**, 135 (2005).
[20] I. Muševič, M. Škarabot, U. Tkalec, M. Ravnik, and S. Žumer, Science **313**, 954 (2006).

[21] M. Ravnik, M. Škarabot, S. Žumer, U. Tkalec, I. Poberaj, D. Babič, N. Osterman, and I. Muševič, Phys. Rev. Lett. **99**, 247801 (2007).
[22] M. Škarabot, M. Ravnik, S. Žumer, U. Tkalec, I. Poberaj, D. Babič, N. Osterman, and I. Muševič, Phys. Rev. E **76**, 051406 (2007).
[23] U. Ognysta, A. Nych, V. Nazarenko, I. Muševič, M. Škarabot, M. Ravnik, S. Žumer, I. Poberaj, and D. Babič, Phys. Rev. Lett. **100**, 217803 (2008).
[24] M. Škarabot, M. Ravnik, S. Žumer, U. Tkalec, I. Poberaj, D. Babič, N. Osterman, and I. Muševič, Phys. Rev. E **77**, 031705 (2008).
[25] M. Ravnik and S. Žumer, Soft Matter **5**, 269 (2009).
[26] F. R. Hung, Phys. Rev. E **79**, 021705 (2009).
[27] M. Ravnik and S. Žumer, Liq. Cryst. **36**, 1201 (2009).
[28] S. Dhakal, F. J. Solis, and M. Olvera de la Cruz, Phys. Rev. E **86**, 011709 (2012).
[29] V. Koning, T. Lopez-Leon, A. Darmon, A. Fernandez-Nieves, and V. Vitelli, Phys. Rev. E **94**, 012703 (2016).
[30] G. Napoli and L. Vergori, Phys. Rev. E **94**, 020701(R) (2016).
[31] A. M. Sonnet and E. G. Virga, Soft Matter **13**, 6792 (2017).
[32] A. H. Lewis, D. G. A. L. Aarts, P. D. Howell, and A. Majumdar, SIAM J. Appl. Math. **77**, 1851 (2017).
[33] A. H. Lewis, D. G. A. L. Aarts, P. D. Howell, and A. Majumdar, Studies App. Math. **138**, 438 (2017).
[34] Y. Wang, P. Zhang, and J. Z. Y. Chen, Phys. Rev. E **96**, 042702 (2017).
[35] Y. Wang, P. Zhang, and J. Z. Y. Chen, Soft Matter **14**, 6756 (2018).
[36] P. G. de Gennes and J. Prost, *The Physics of Liquid Crystals* (Oxford University Press, Oxford, 1993).
[37] L. Onsager, Ann. NY Acad. Sci. **51**, 627 (1949).
[38] R. Pathria, *Statistical Mechanics* (Butterworth Heinemann, Oxford, 1996).
[39] R. F. Kayser and H. J. Raveche, Phys. Rev. A **17**, 2067 (1978).
[40] J. A. Cuesta, C. F. Tejero, and M. Baus, Phys. Rev. A **39**, 6498 (1989).
[41] Z. Y. Chen, Phys. Rev. Lett. **71**, 93 (1993).
[42] X. Yao, H. Zhang, and J. Z. Y. Chen, Phys. Rev. E **97**, 052707 (2018).
[43] J. Z. Y. Chen, Soft Matter **9**, 10921 (2013).
[44] J. Z. Y. Chen, Prog. Polym. Sci. **54-55**, 3 (2016).
[45] D. R. Nelson, *Defects and Geometry in Condensed Matter Physics* (Cambridge University Press, Cambridge, 2002).
[46] M. J. Bowick and L. Giomi, Adv. Phys. **58**, 449 (2009).
[47] A. M. Turner, V. Vitelli, and D. R. Nelson, Rev. Mod. Phys. **82**, 1301 (2010).
[48] Q. Liang, Y. Jiang, and J. Z. Y. Chen, Phys. Rev. E **100**, 032502 (2019).
[49] W.-Y. Zhang, Y. Jiang, and J. Z. Y. Chen, Phys. Rev. Lett. **108**, 057801 (2012).
[50] W.-Y. Zhang, Y. Jiang, and J. Z. Y. Chen, Phys. Rev. E **85**, 061710 (2012).
[51] Q. Liang, S. Ye, P. Zhang, and J. Z. Y. Chen, J. Chem. Phys. **141**, 244901 (2014).
[52] S. Ye, P. Zhang, and J. Z. Y. Chen, Soft Matter **12**, 5438 (2016).